

Landslides (2021) 18:105–123
 DOI 10.1007/s10346-020-01491-7
 Received: 28 November 2019
 Accepted: 15 July 2020
 Published online: 2 August 2020
 © Springer-Verlag GmbH Germany
 part of Springer Nature 2020

Danqing Song · Xiaoli Liu · Jin Huang · Jianmin Zhang

Energy-based analysis of seismic failure mechanism of a rock slope with discontinuities using Hilbert-Huang transform and marginal spectrum in the time-frequency domain

Abstract An energy-based identification method is proposed to investigate the seismic failure mechanism of landslides with discontinuities. The proposed method was verified by using shaking table tests on a rock slope with discontinuous structural planes. The results show that it is feasible to analyze the seismic failure mechanism of the slope by using Hilbert-Huang transform (HHT) and marginal spectrum based on seismic Hilbert energy. Earthquake energy mainly concentrating in the low-frequency components (15–17 Hz) and high-frequency components (20–40 Hz), in Hilbert energy spectrum and the marginal spectrum, respectively, suggests that they can identify the overall and local dynamic response of the slope, respectively, in combination with the Fourier spectrum analysis. In addition, the analyses of marginal spectrum can better clarify the slope dynamic damage process from the energy-based perspective, including no seismic damage stage, local damage stage, and sliding failure stage. The difference of seismic Hilbert energy between slip mass and sliding body causes their different seismic responses. The seismic failure mechanism of the landslide is identified from the energy-based perspective: the seismic Hilbert energy in 20–40 Hz mainly induces the local damage of the slope above the topmost bedding structural plane, and local failure develops first at the platform, under 0.297 g; the surface slope gradually forms a sliding body with the accumulation of local damage, and the seismic Hilbert energy in 15–17 Hz further promotes the landslide subject to 0.446 g.

Keywords Seismic failure mechanism · Seismic Hilbert energy · HHT · Marginal spectrum · Rock slope · Discontinuities

Introduction

A remarkable consistency can be found between the global distribution of landslide zones and seismic zones (Chang et al. 2006; Zhang and Huang 2018); this finding sufficiently suggests that earthquakes have a significant effect on the stability of landslides. Recent earthquakes have demonstrated that the sliding and collapse of a slope during such large-scale events represent significant seismic hazards, for example, the 2008 Wenchuan earthquake and the 2010 Yushu earthquake in China (Qi et al. 2010; Xu et al. 2013; Huang and Li 2014). In addition, multitudes of joints, which constitute structural planes, are widely distributed throughout rock masses (Wu et al. 2014; Jiang et al. 2015; Song et al. 2018a, b; Chen et al. 2020), which can significantly influence the seismic failure mechanism of rock masses (Fan et al. 2016; Song et al. 2018a). Therefore, the seismic failure mechanism of rock masses should be paid much more attention due to the complex geological structure (Jiang et al. 2015; Fan et al. 2016; Song et al. 2018c).

Seismic damage has close relationship between amplitude, frequency, and duration of the vibration. However, it cannot reflect

the overall vibration and damage results by using a specific ground motion parameter that reflects a particular property (Peláez et al. 2005; Song et al. 2020). The occurrence of earthquake-induced landslides is closely related to the peak ground acceleration (PGA), the frequency components, the energy, the directivity of seismic waves, etc. (Lenti and Martino 2012). Weak structural planes in rock slopes have a significant impact on the dynamic stability of slopes, which results in the complexity of the dynamic response of slopes (Jiang et al. 2015; Fan et al. 2016). Hence, the dynamic response characteristics of slopes can be evaluated difficultly by using PGA in the time domain. The existing researches were mostly based on the acceleration response of slopes (Yin et al. 2009; Fan et al. 2018; Song et al. 2018a). However, it is rare to investigate the slope seismic response from the perspective of the characteristic parameters and the physical quantity of slopes; in particular, the effects of seismic energy in rock masses on their dynamic stability were ignored (Chen et al. 2013). Moreover, earthquake energy is an essential trigger of earthquake-induced landslides (Chen et al. 2013; Fan et al. 2016). Therefore, the seismic failure mechanism of rock slopes with weak structural planes needs to be investigated from the energy-based perspective (Fan et al. 2017).

In recent years, some energy-based energy methods have been proposed to investigate the rock slope stability (Chen et al. 2013; Peng et al. 2015; Meng et al. 2016; Fan et al. 2017; Song et al. 2019). Kokusho et al. (2011, 2014) proposed an energy approach to evaluate the travel distance of debris in the process of slope failure caused by earthquakes using seismic energies of slopes. Peng et al. (2015) investigated the relationship between the damage of coal rocks and energy dissipation and release by using triaxial compression tests. Chen et al. (2015) studied the correlation between the radiation energy of rockburst and its intensity according to the radiation energy characteristics of rockburst. Munoz et al. (2016) used a new energy-based brittleness index to study drilling performance through rock strength characteristics. However, currently, there is little study on the relationship between the seismic energy and the seismic failure mechanism of earthquake-induced landslides from a perspective of the energy-based method.

Due to the typical non-stationary random characteristics of earthquake signals, time domain and frequency domain analysis cannot process these signals accurately. Hence, the time-frequency analysis method has attracted the attention of many scholars (Pai and Palazotto 2008; Fan et al. 2017; Song et al. 2020). Fast Fourier transform (FFT) and wavelet transform (WT) are commonly used to process non-stationary random signals. FFT can only provide the energy distribution with the frequency of wave, but not simultaneously clarify the overall and local characteristics in the time and frequency domains. The WT can clarify the front-back

asymmetry, but its frequency resolution is poor, especially in the low-frequency domain (Wang et al. 2013). As the preferred method to process seismic signals, HHT has an excellent time-frequency resolution, when the non-stationary signal is described in the time-frequency domain (Jia 2008; Veltcheva and Soares 2016; Fan et al. 2017). HHT can overcome the limitations of conventional signal processing methods (Pai and Palazotto 2008; Wang et al. 2013; Fan et al. 2017). Due to the prominent time-frequency localization ability, HHT has been widely used in the fields of structure damage detections (Roveri and Carcaterra 2012; Song et al. 2020), ocean engineering (Veltcheva and Soares 2016), earthquake studies (Fan et al. 2016), etc. Jia (2008) investigated the fatigue damage of fixed offshore structures by the HHT method. Han et al. (2016) studied the damage process of carbon-fiber-reinforced plastic by using HHT. Cao et al. (2017) investigated the seismic damage evolution process within a complex site with tilting strongly weathered layer by using HHT. Fan et al. (2017) investigated the dynamic failure mechanism of rock slope with a weak zone from a perspective of the energy-based method by using HHT. The existing studies demonstrated that the HHT method is adaptive and highly efficient in processing seismic signals. However, limited research has been conducted regarding the seismic failure mechanism of rock masses with weak structural planes by using the energy-based method, in particular, the applicability of seismic Hilbert energy spectrum and marginal spectrum to the study of the overall or local deformation of landslides should be further discussed.

In this work, an energy-based identification method of the seismic failure mechanism of landslides with discontinuities is proposed based on the HHT and marginal spectrum. To illustrate the applicability of the energy-based method in evaluating the seismic response characteristics and failure mechanism of landslides under seismic excitation, the Lijiang slope of Jinshajiang bridge is taken as an example, and large-scaled shaking table tests are conducted on a rock slope with discontinuous structural planes. HHT is applied to measure the seismic energy response of different slope parts. The applicability of seismic Hilbert energy spectrum and marginal spectrum to analyze the dynamic response characteristics of the landslide is also discussed in depth. The seismic damage development process and failure mechanism of the landslide are clarified by using seismic Hilbert energy, which is meaningful for further study of the seismic failure mode of the landslide from the perspective of energy-based transmission characteristics.

Energy-based method of seismic slope damage

HHT and the theory of marginal spectrum

Huang et al. (1998) proposed a new signal processing method, namely the HHT method, which mainly includes empirical mode decomposition (EMD) method and Hilbert spectral analysis (HSA). HHT method focuses on the intrinsic mode function (IMF) using the EMD method. The EMD method is an adaptive data processing or mining method, which can decompose the signal into a finite number of multi-order IMFs. It is very suitable for the processing of nonlinear time series, which is essentially the smoothing processing of data series or signals (Huang et al. 1998, 1999). Before the HSA, the EMD method has been the important pretreatment step. The specific steps of the EMD method are as follows. First, the local extreme value of time history curve $X(t)$

should be searched and found. The local maximum and minimum points are connected by the difference of cubic spline curves to obtain the maximum envelope and minimum connection curve. Second, the instantaneous average value $m_1(t)$ is achieved by averaging the extreme connection curves. Finally, the new sequence $h_1(t)$ with removing the low frequency is obtained by using the original sequence $X(t)$ minus the instantaneous average $m_1(t)$. The flowchart for the EMD approach is given in Fig. 1. In particular, the two conditions of IMF are as follows: first, at any time point, the mean value between the upper and lower envelope defined by the local extremum point is 0; second, in the whole time domain of the original signal, the number of the extremum and zero-crossing is 0 or less than 1. If $h_1(t)$ meets the above two conditions, then $h_1(t)$ is the IMF; otherwise, $h_1(t)$ will be screened again until the Eqs. (1) and (2) are satisfied, as follows:

$$h_1(t) = X(t) - m_1(t) \quad (1)$$

$$h_{11}(t) = h_1(t) - m_{11}(t) \quad (2)$$

Repeat the screening process k times until the $h_{1k}(t)$ is a certain IMF, and the $h_{1k}(t)$ is as follows:

$$h_{1k}(t) = h_{1(k-1)}(t) - m_{1k}(t) \quad (3)$$

where the first IMF is denoted as $c_1(t)$. The $c_1(t)$ is separated from the original sequence.

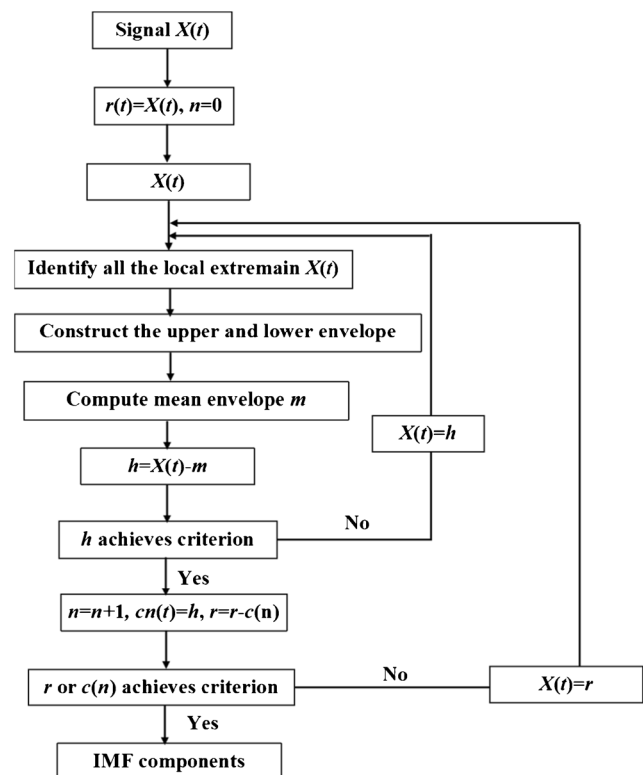
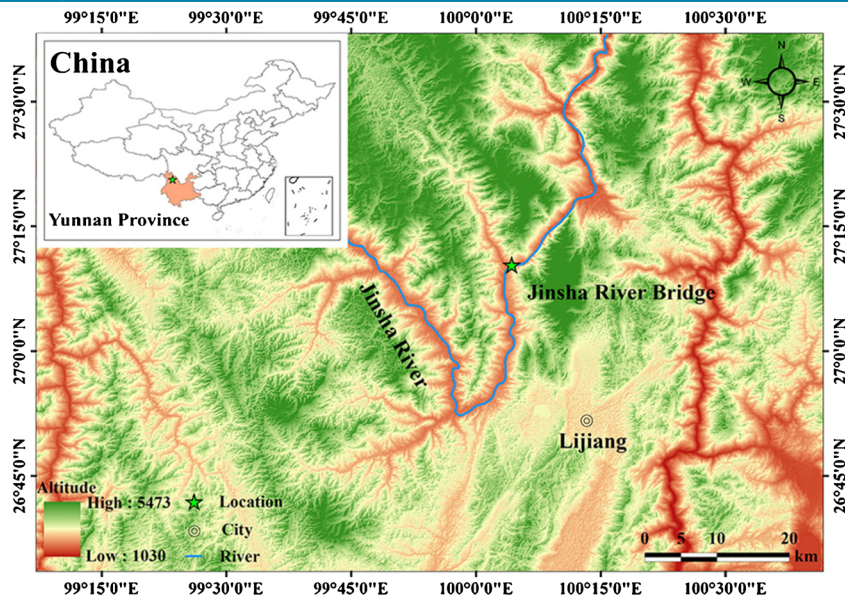
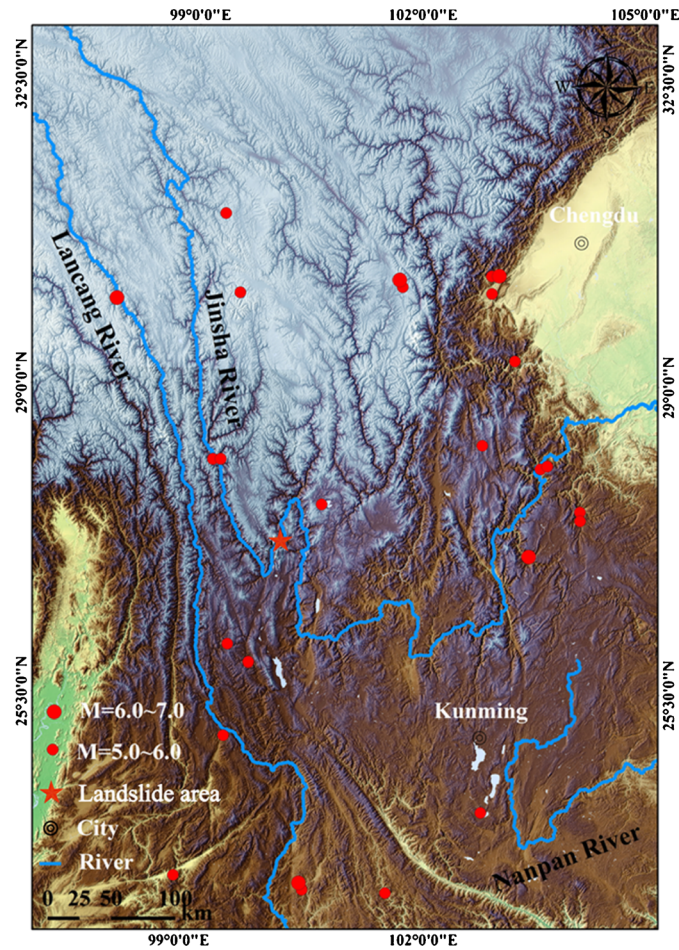


Fig. 1 Flowchart for EMD approach (Zhang 2006)



(a)



(b)

Fig. 2 Overview of the study area: **a** location of the study area; **b** seismic activity distribution map near the study area in the last 6 years

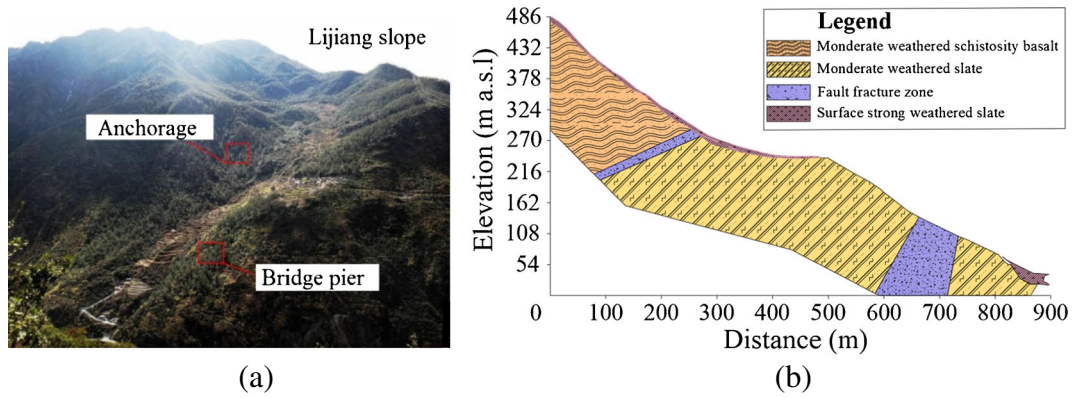


Fig. 3 The topographic and geological conditions of the Lijiang slope: **a** the topography of the slope; **b** the geological section of the slope (Song et al. 2018a)

$$c_1(t) = h_{1k}(t) \tag{4}$$

The $h_{1k}(t)$ is defined as $c_1(t)$, that is, the first IMF (IMF₁). IMF₁ is derived from the original signal, that is,

$$r_1(t) = X(t) - c_1(t) \tag{5}$$

As a new signal, $r_1(t)$ was used to repeat the above steps to select IMF, until the original sequence $X(t)$ was decomposed into n IMF and a residue r_n . The original signal $X(t)$ is the sum of all IMFs plus the final residue, that is,

$$X(t) = \sum_{j=1}^n c_j(t) + r_n(t) \tag{6}$$

The HHT $Y(t)$ of any time series $c(t')$ can be denoted as

$$Y(t) = \frac{1}{\pi} P \int_{t-t'}^{t+t'} \frac{c(t')}{t-t'} dt' \tag{7}$$

where $Y(t)$ and $C(t)$ form a complex conjugate pair, and P represents the Cauchy principal value. Then, the analytical signal $z(t)$ is obtained as

$$z(t) = C(t) + iY(t) = a(t)e^{i\theta(t)} \tag{8}$$

where the instantaneous phase $\theta(t)$ and amplitude $a(t)$ are found as

$$\theta(t) = \arctan \sqrt{Y(t)/C(t)} \tag{9}$$

$$a(t) = \sqrt{c^2(t) + Y^2(t)} \tag{10}$$

where the $\theta(t)$ is defined as

$$\omega(t) = \frac{d\theta(t)}{dt} \tag{11}$$

It can be found that the $a(t)$ and $\omega(t)$ are time function. The Hilbert-Huang spectrum, that is, the $H(\omega, t)$, can be defined as

$$H(\omega, t) = \text{Re} \sum_{j=1}^n a_j(t) e^{i\int \omega_j(t) dt} \tag{12}$$

The HHT marginal spectrum, $h(\omega)$, is defined as the integration of the $H(\omega, t)$ on the time axis. The $h(\omega)$ is defined as

$$h(\omega) = \int_0^T H(\omega, t) dt \tag{13}$$

The Hilbert spectrum of the original signal can be obtained according to the Hilbert transform (HT), and then, the corresponding marginal spectrum of the original signal will be acquired.

+The Hilbert spectrum shows simultaneously the time, instantaneous frequency, and wave amplitude of the original wave in three-dimensional coordinates, which represents the distribution of seismic Hilbert energy of the original wave as well. Each instantaneous frequency owns a certain energy, and its amplitude can be obtained by the marginal spectrum. The marginal spectrum can be used to measure the contribution of each frequency value to the total Hilbert energy contribution and corresponds to a Hilbert energy density at

Table 1 Physico-mechanical parameters of material parameters of the slope

Type	Physical and mechanical parameters	Density $\rho/\text{kN/m}^3$	Poisson ratio μ	Dynamic elastic modulus E/GPa	Friction angle ϕ (°)	Cohesive force c (kPa)
Lijiang slope	Rock mass	28.5	0.30	10.0	49.0	2300
	Structural surface	/	/	/	36.1	1200
Model slope	Rock mass	28.5	0.3	0.025	49.0	4.8
	Structural surface	/	/	/	36.1	5.75

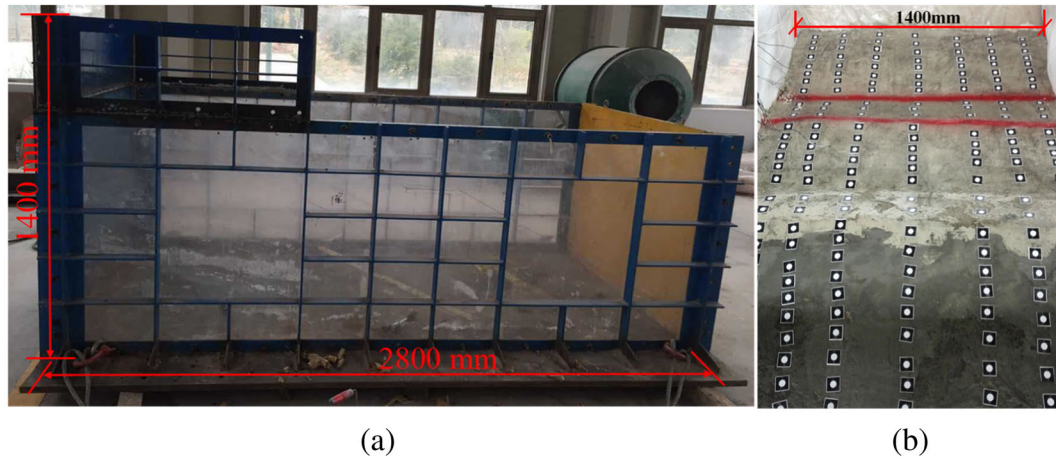


Fig. 4 The test system: **a** experimental tank; **b** scaled model

certain a frequency ω . The Hilbert marginal spectrum obtained by HHT represents the distribution of the energy amplitude of the seismic wave signal on the frequency axis, which means the cumulative Hilbert energy of the original wave over the entire data span in the form of probability. In the frequency domain, the damage characteristics in the engineering entity structure can be characterized in the frequency domain from the perspective of energy using the Hilbert marginal spectrum.

Identification method for seismic failure of rock slopes

Rock slopes may suffer dynamic damage under seismic excitation. The seismic damage of any positions in the slope will cause that the vibration energy of the slope body cannot be transmitted at the slope part, and the energy dissipation will result in the abrupt change or violent fluctuation of MSA (Li et al. 2012; Fan et al. 2016, 2017). The

above-mentioned IMF components were carried out HHT to obtain the instantaneous frequency spectrum and the corresponding marginal spectrum with the change of time. Marginal spectrum of each measuring point in the slope was analyzed; if the PMSA (peak marginal spectrum amplitude) increases with a slight variation from the bottom slope to the top slope, this phenomenon suggests that no dynamic damage appears within the slope. However, when the seismic intensity reaches a certain value, the PMSA of any part has an abrupt change, and the PMSA above this part is stable within a small range. This phenomenon indicates that there is a different seismic response at some parts of the slope from the others, and seismic damage occurs in this part, from the perspective of damage analysis. Therefore, for the slope with discontinuous structural planes, the slope will produce seismic damage due to the continuous earthquake excitation. The slope seismic damage will directly destroy the structural integrity of

Table 2 The similarity ratios of the model. Here, L , ρ , and a are controlling parameters

No.	Parameters	Dimension analysis	Dimensionless (π) item	Similarity ration
1	Density (ρ)	$[M] [L]^{-3}$	Controlling parameter	$C_\rho = 1$
2	Physical dimension (L)	$[L]$	Controlling parameter	$C_L = 400$
3	Elasticity modulus (E)	$[M] [L]^{-1} [T]^{-2}$	$\pi_E = E/\rho L$	$C_E = C_\rho C_L = 400$
4	Poisson's ratio (μ)	-	1	$C_u = 1$
5	Cohesive force (c)	$[M] [L]^{-1} [T]^{-2}$	$\pi_c = c/L$	$C_c = C_L = 400$
6	Internal friction angle (ϕ)	-	1	$C_\phi = 1$
7	Stress (σ)	$[M] [L]^{-1} [T]^{-2}$	$\pi_\sigma = \sigma/L$	$C_\sigma = C_L = 400$
8	Strain (ε)	-	1	$C_\varepsilon = 1$
9	Time (t)	$[T]$	1	$C_t = 1$
10	Frequency (ω)	$[T]^{-1}$	$\pi_\omega = \omega/t^{-1}$	$C_\omega = C_t^{-1} = 1$
11	Displacement (s)	$[L]$	$\pi_s = s/\rho La$	$C_s = C_\rho C_L C_a = 400$
12	Velocity (v)	$[L] [T]^{-1}$	$\pi_v = v/\rho La$	$C_v = C_\rho C_L C_a = 400$
13	Acceleration (a)	-	Controlling parameter	$C_a = 1$
14	gravitational acceleration (g)	$[L] [T]^{-2}$	$\pi_g = g/a$	$C_g = C_a = 1$
15	Damping ration (λ)	-	1	$C_\lambda = 1$

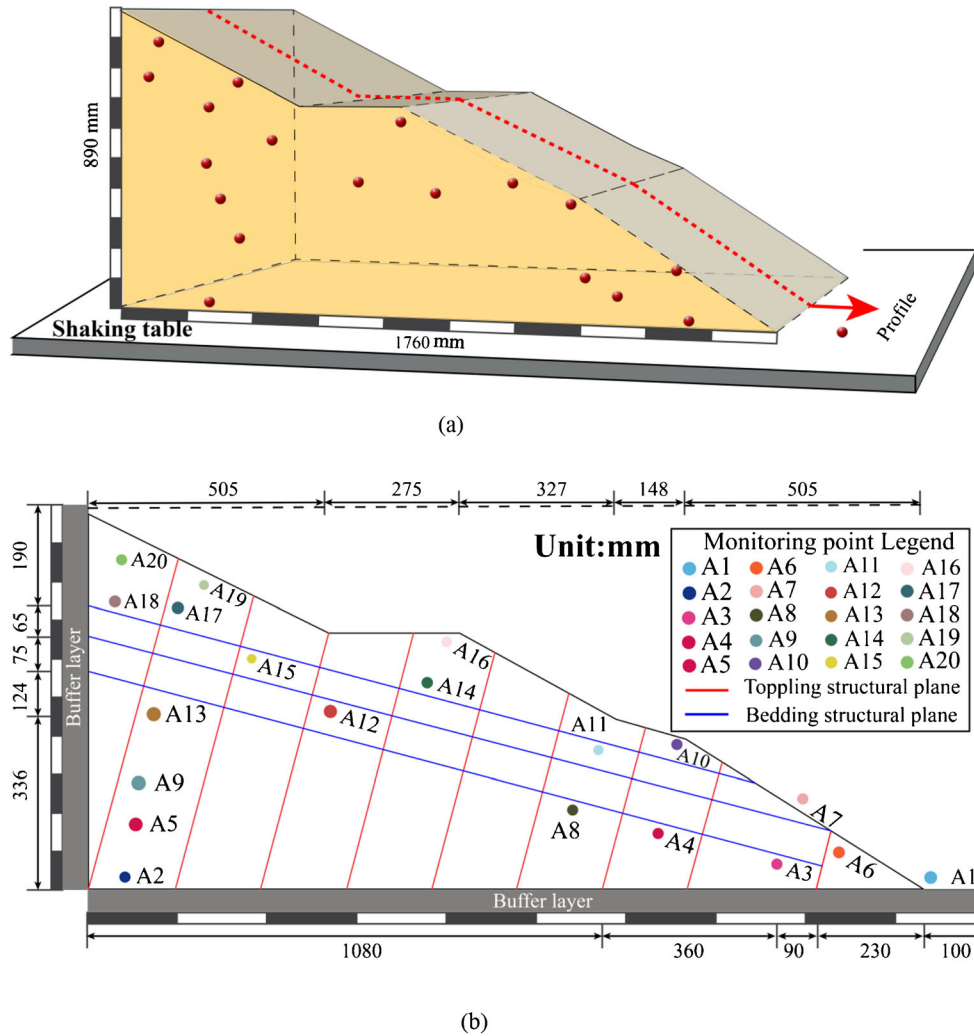


Fig. 5 The test model: a schematic diagram of the model; b cross-sectional illustration of the model and the layout of accelerometer monitoring points

slope, with the PMSA above the damaged part of the slope changing abruptly undoubtedly. The study steps of the slope failure mechanism using the Hilbert marginal spectrum are as follows: first, the acceleration time history of all measuring points was broken down by using EMD to get many IMFs. Second, HHT was performed on each IMF to obtain the corresponding instantaneous frequency curves and marginal spectrum. Third, the seismic Hilbert energy distribution of

the slope was determined according to the Hilbert marginal spectrum of measuring points, and the damage location of the slope was further inferred. Finally, the seismic damage evolution process and mechanism of the slope are clarified according to the change rule of the PMSA at different parts in the slope from the energy-based identification method, in combination with the dynamic damage phenomena.

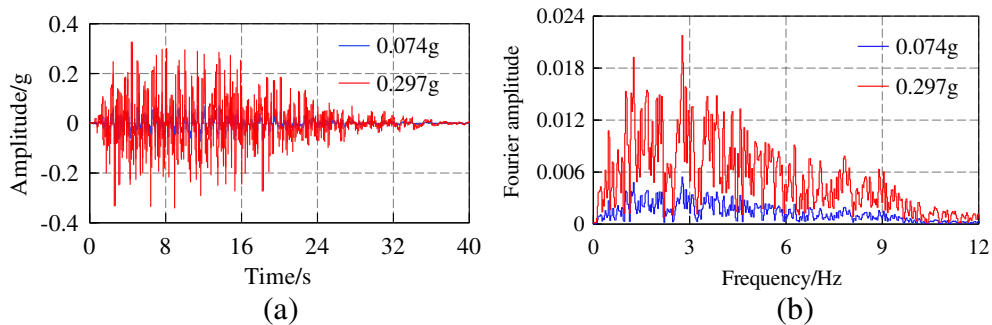


Fig. 6 Input artificial synthetic waves: a time history; b Fourier spectrum

Table 3 The test loading sequence

Vibration direction	z	x	z	x	z	x	z	x
No.	1	2	3	4	5	6	7	8
Amplitude (g)	0.074	0.074	0.148	0.148	0.297	0.297	0.446	0.446

Application of the energy-based identification method in a landslide under seismic excitation

Case study

The study area is located in the transition zone between the southeastern edge of the Yunnan-Kweichow plateau and the Qinghai-Tibet plateau in southwest China. Strong neotectonics movements characterize the area, and several faults pass through the region. The study area is the deep valley landform of the Jinsha River. The valley is dominated by a V-type valley shape, and there are no developed terraces. The Jinshajiang bridge in tiger leaping gorge is located at the junction of Lijiang city and Diqingzhou Shangri-la county, Yunnan province, China (Fig. 2a). The bridge site is located in the area of tectonic denudation canyon; under the influence of regional tectonics, the dynamic metamorphism of each rock formation near the bridge site is active. In recent years, the distribution of seismic activities near the study area is shown in Fig. 2b. In Fig. 2b, the location refers to the Jinsha river bridge.

Due to the frequent earthquakes in the study area, the stability of rock slopes has a significant impact on the Jinsha river bridge. Hence, the seismic stability of rock slopes with complex geological structures has been a significant problem. To investigate the seismic stability of rock slopes, taking a natural bank slope, that is, the Lijiang slope as an example, the topography of the Lijiang slope is shown in Fig. 3a. The gradient of the Lijiang slope is about 40°. Lijiang bank mainly has three bedding weak structural planes and many toppling weak structural plane. The topography of the slope and its geological profile are shown in Fig. 3b. The physical and mechanical parameters of the rock and weak structural surfaces in the slope needed for constructing the model were obtained according to a series of laboratory tests, as listed in Table 1.

Shaking table tests

The bi-directional electric servo shaking table is controlled by a direct control system and input vibration wave, and the horizontal and vertical seismic loads can be simulated using the shaking

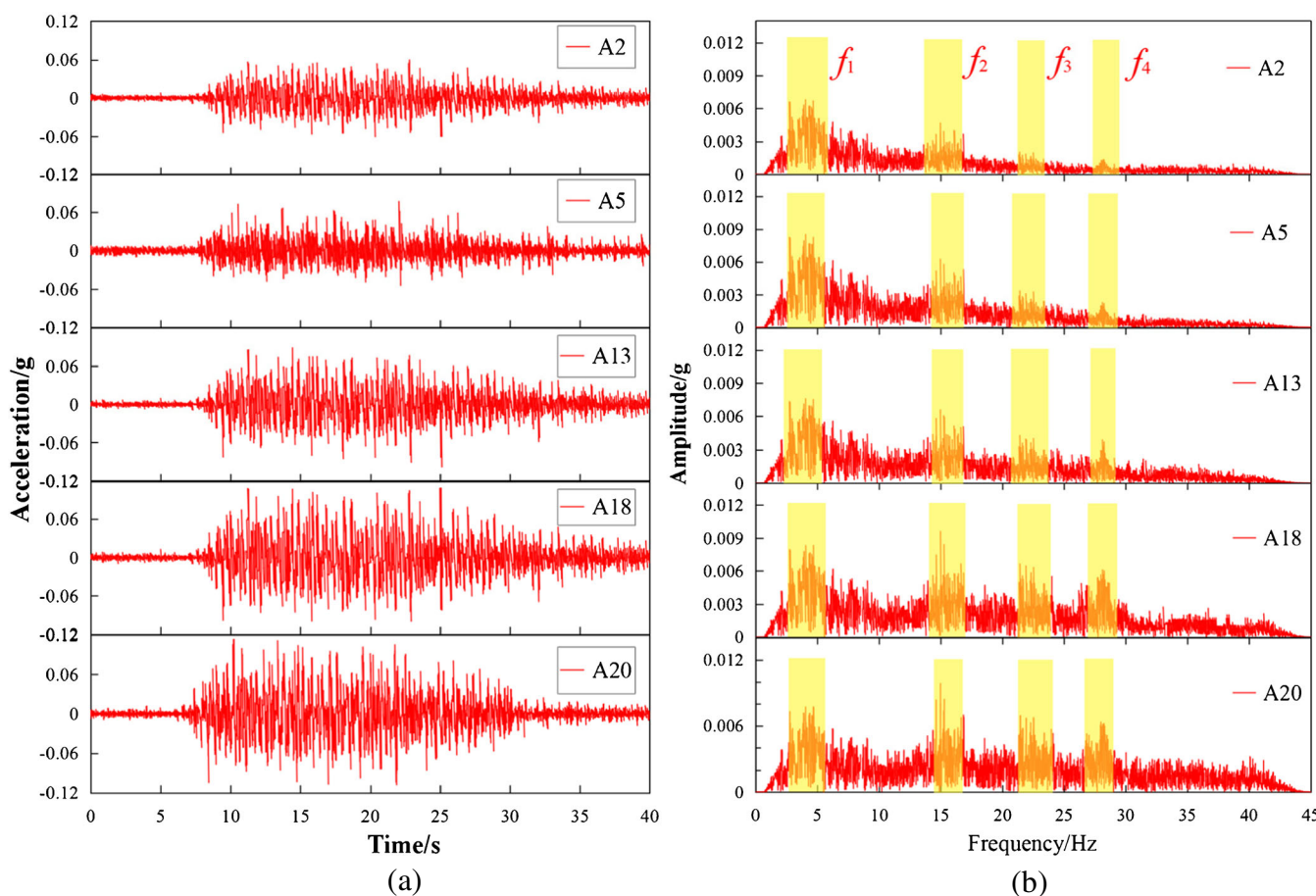
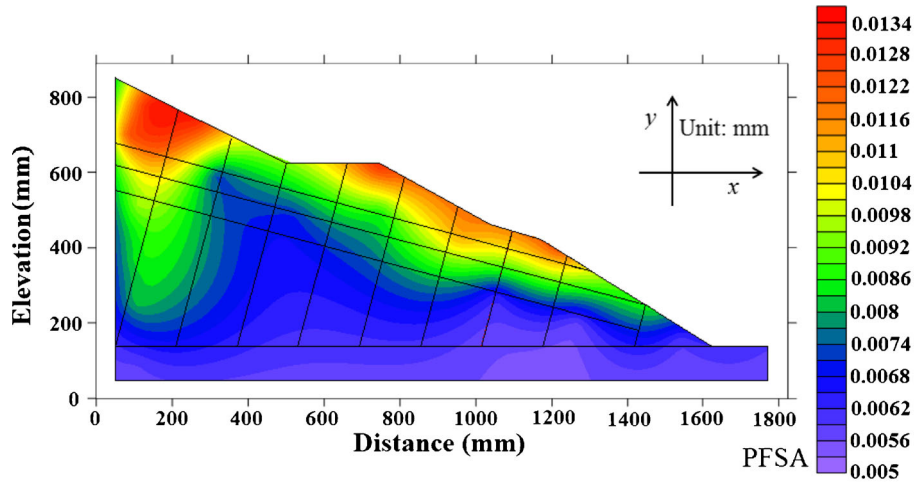
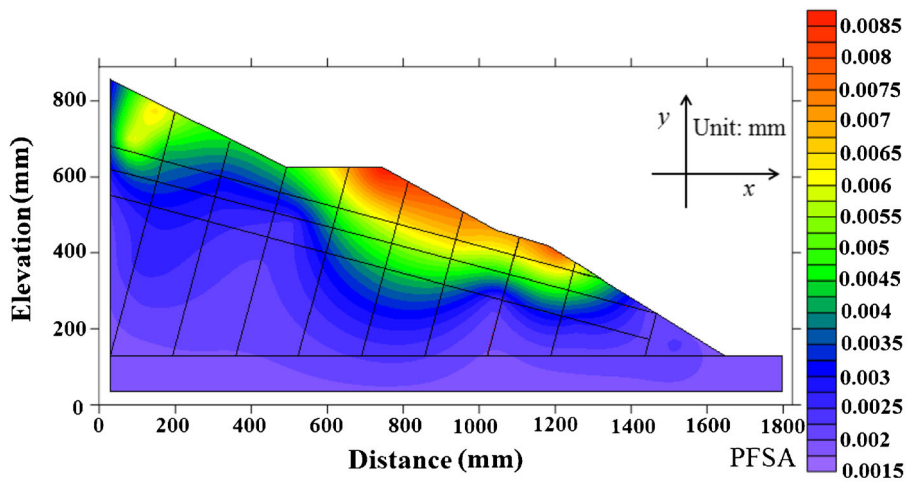


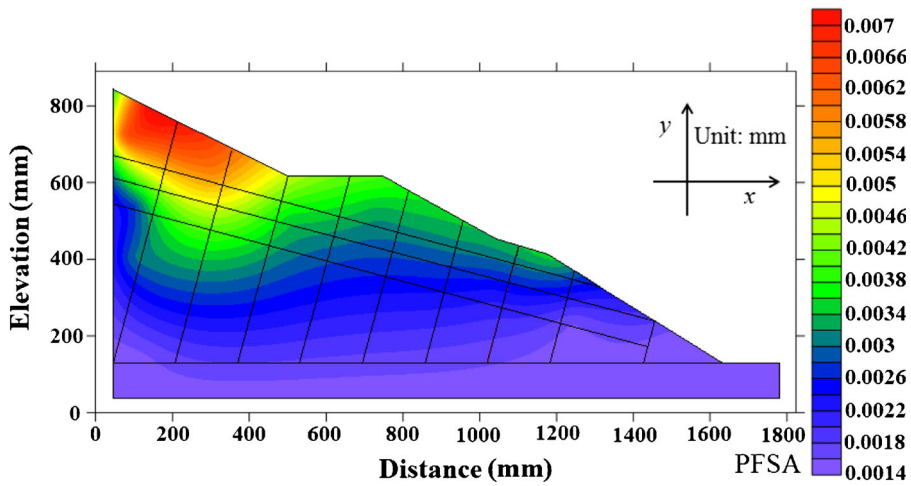
Fig. 7 The measuring points when input AS wave (0.074 g) in x-direction: a acceleration-time curve; b Fourier spectra



(a)



(b)



(c)

Fig. 8 Distribution of PFSA when input in x -direction (0.148 g): a during 14–16 Hz; b during 22–24 Hz; c during 27–29 Hz

table. The vibration frequencies of the shaking table are 0.1–70 Hz in horizontal and 0.1–50 Hz in vertical, respectively. The maximum acceleration of the input seismic wave is 1.7 g and 1.2 g in horizontal and vertical, respectively. An experimental tank with interior dimensions of $2.8 \times 1.4 \times 1.4$ m was developed for the tests (Fig. 4a). In the tests, the model geometry (L), mass density (ρ), and seismic acceleration (a) were regarded as the basic dimension, with scaling $C_L = 400,000$, $C_\rho = 1,000$, and $C_a = 1,000$, respectively. To simulate the prototype slope in the model test, the law of similitude is applied, based on Buckingham's π theorem of similarity, which is based on dimensional analysis and gives the transformation from a function of dimensional parameters to a function in the present study (Fan et al. 2016). The similarity constant of physical quantities in the tests is as shown in Table 2. Lijiang slope is the prototype of this model (Fig. 3). By the similarity calculation, the material parameter of the model can be calculated. The μ , c , ϕ , G , and ρ are 0.30, 0.048 MPa, 49° , 25 MPa, and 28.5 kN/m^3 , respectively. Water, steel, slag, sand, and gypsum were used to simulate the rock in the model, and their

ratios are 2.1:5:4:1.3. As the model is large, it is difficult to construct the model by integral casting, and prefabricated blocks are used to build the model. After the similarity ratio calculation, it is found that the physical and mechanical parameters of gray board are close to the structural surface of the model, which is used as the simulated material. The model slope is 0.89 m high and 1.86 m long, as shown in Fig. 4b. Prefabricated blocks were stacked in four layers to construct the model slope. According to the direct reduction tests, gray paperboard was adopted to simulate the structural surfaces. The model slope is shown in Fig. 4b.

Twenty-three three-component capacitive accelerometers were embedded inside the model (Fig. 5). XTDIC 3D optical deformation measurement system was used to collect the displacement data of slope surface. Three measures were taken in these tests to minimize the impacts of reflections of seismic waves from the boundaries of the model box. First, transparent rubber cushion is set at the bottom of the model box, which can play a good cushioning role in the test process and avoid friction and slip between the model slope and the model box. Second, a buffer

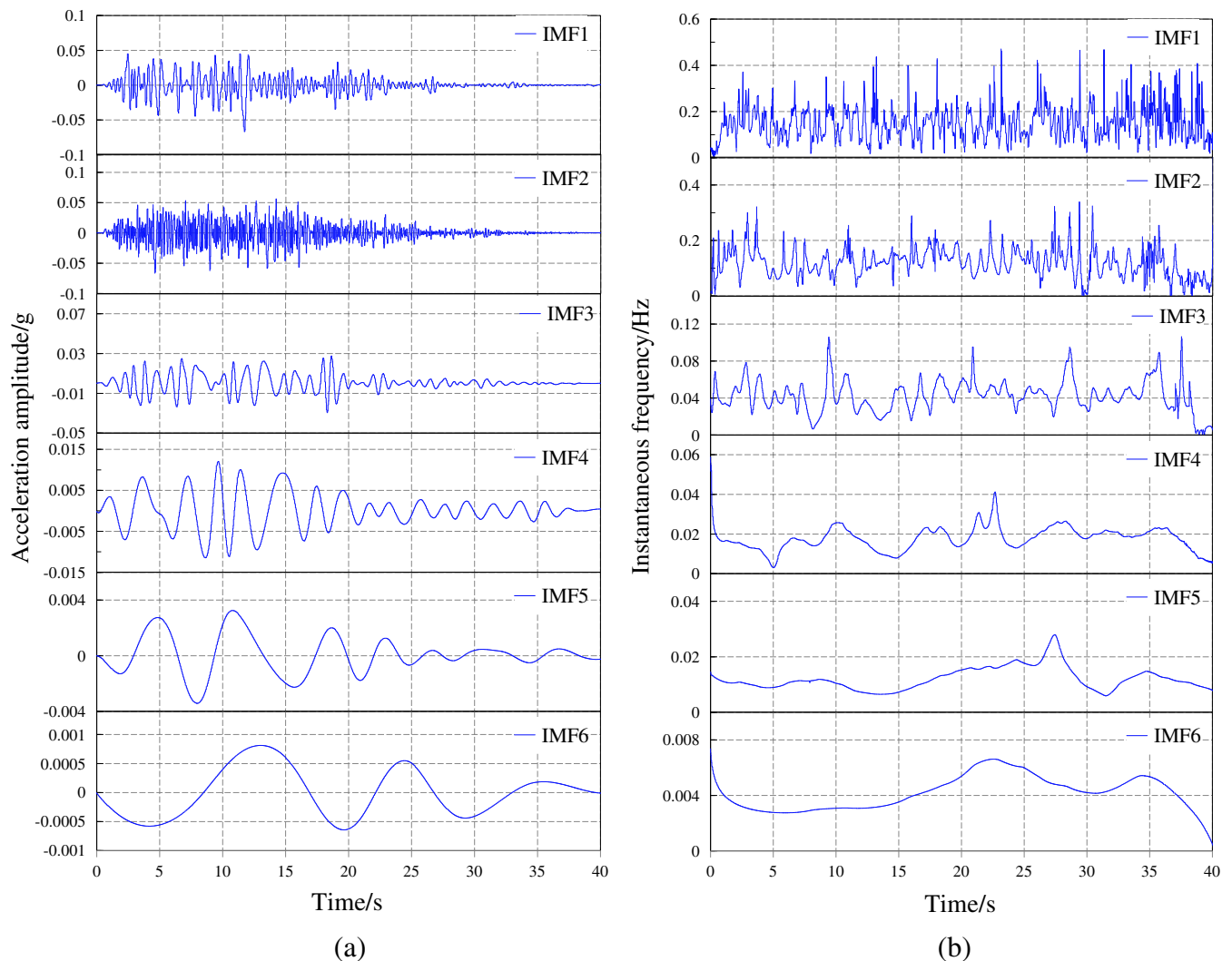


Fig. 9 EMD results of the input AS wave (0.074 g): **a** IMF1–6; **b** the corresponding instantaneous frequencies of the IMFs

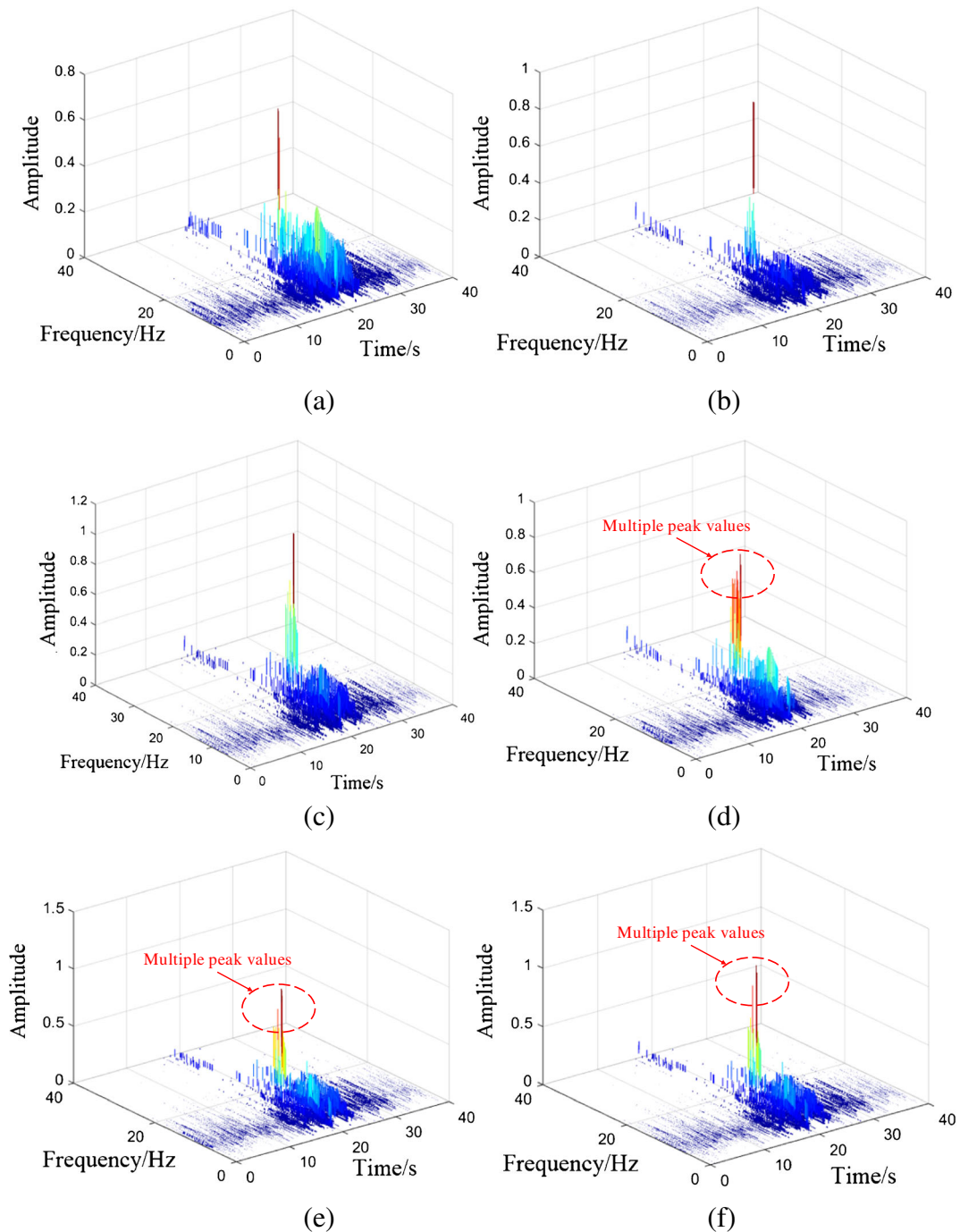


Fig. 10 Seismic Hilbert energy spectra of measuring points at the internal slope and the surface slope when input AS wave in x -direction (0.074 g): a A2; b A7; c A13; d A10; e A16; f A18

layer was set at the bottom of the scaled model, and its material is the same as the model, whose purpose is to allow free deformation of the model boundary, and also simulate the infinite boundary conditions in the model. Third, the acceleration sensors are arranged in the middle section of the model to minimize the adverse influence of the model box boundary on the data collection. An artificial synthetic (AS) wave was used in the tests; taking the input AS waves (0.074 g and 0.297 g) as

examples, their corresponding acceleration-time curve and Fourier spectrum are shown in Fig. 6. Two seismic excitation loading directions were applied in the tests: the vertical or z -direction and the horizontal or x -direction. The seismic wave loading sequences are shown in Table 3. The original acceleration-time history collected in the tests needs to be pre-processed by using MATLAB, mainly including filtering, baseline calibration, and smoothing processing.

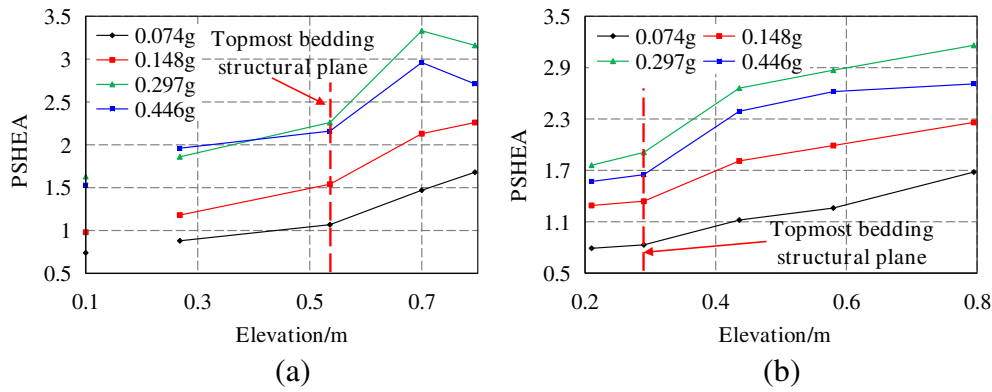


Fig. 11 The change rule of PSHEA with elevation when input in *x*-direction: **a** inside the slope; **b** near the slope surface

Energy-based identification for slope damage

Analysis of seismic Hilbert energy spectrum

To investigate the seismic response of the slope in the time-frequency domain, the relationship between frequency components and the dynamic response of the slope should be discussed first. Taking input AS wave in the *x*-direction as an example, the acceleration-time histories and corresponding Fourier spectra of the typical monitoring points inside the slope subject to 0.074 g are shown in Fig. 7. Four predominant frequencies can be identified in Fig. 7, but the f_1 is similar to that of the input AS wave (Fig. 6b); hence, the f_2 , f_3 , and f_4 are the natural frequencies of the slope. Taking input 0.148 g AS wave as an example, the peak Fourier spectra amplitude (PFSA) of each natural frequency are shown in Fig. 8. The PFSA of the all monitoring points is extracted, and the distribution cloud picture of the PFSA is drawn by using Surfer 10 software. The color code and contour line in Fig. 8 represent the distribution of the PFSA values. Figure 8 shows that the low-frequency components (14–16 Hz) and the high-frequency components (> 20 Hz) mainly induced the overall and local dynamic response of the slope body above the topmost bedding structural plane (surface slope), respectively.

The EMD results of AS wave under 0.074 g and their corresponding instantaneous frequencies are shown in Fig. 9. It can be found that the first six IMFs (IMF1-IMF6) almost contain all

amplitude components of the original seismic wave. The Hilbert energy spectrum of the original signal was obtained by summarizing all the Hilbert spectra of IMFs. The propagation characteristics of the seismic energy of the slope in the time-frequency domain can be clarified according to the analyses of the seismic Hilbert energy. The seismic Hilbert energy spectrum of the typical monitoring points when input in *x*-direction subject to 0.074 g is shown in Fig. 10. Compared with the Fig. 10a–c and d–f, both the shape and peak value of seismic Hilbert energy spectrum of the surface slope (above the topmost structural plane) changed significantly, compared with that of the internal slope (below the topmost structural plane). The frequency components near the peak value of Hilbert energy spectrum of the surface slope have become more abundant when the seismic wave pass through the topmost structural plane, and the seismic Hilbert energy spectrum gradually developed from a single peak in Fig. 10a–c to multiple peaks in Fig. 10d–f. It can be found that seismic Hilbert energy mainly distributes in 15–22 s and 10–20 Hz, on the time axis and on the frequency axis, respectively. In particular, the peak seismic Hilbert energy amplitude (PSHEA) occurs in the 15–18 Hz, which indicates that the 15–18 Hz has an impact on the energy distribution of waves in the slope. This phenomenon suggests that the bedding structural plane has a magnifying effect on the energy propagation of seismic waves, but has less influence on the time and frequency

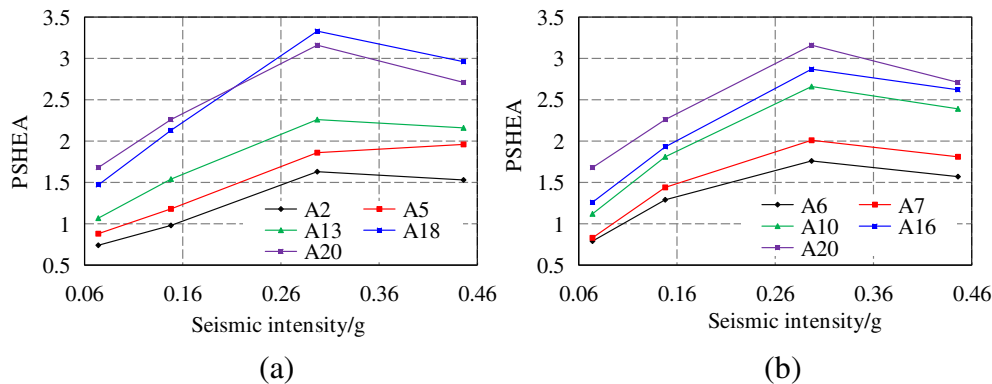


Fig. 12 The change rule of PSHEA with seismic intensity when input in *x*-direction: **a** inside the slope; **b** near the slope surface

of the peak energy of seismic waves. Moreover, the variation rule of PSHEA of typical monitoring points is shown in Fig. 11. Figure 11 shows that the PSHEA increases with the slope elevation, indicating that elevation has an amplification effect on the wave energy transmission of the slope. It is noting that the PSHEA increases rapidly above the topmost structural plane, while that increases slowly below the structural plane, which indicates that the bedding structural plane has an amplification effect in the seismic wave energy transmission.

Combined with the analytical results in Fig. 8, the low-frequency components mainly cause the overall deformation of the slope, suggesting that the seismic Hilbert energy reflects the overall deformation characteristics. In addition, the change of PSHEA with elevation is shown in Fig. 12. The PSHEA increases gradually from 0.074 to 0.297 g, suggesting that no large dynamic deformation occurs in the slope. But the PSHEA decrease from 0.297 to 0.446 g, which indicates that the seismic energy propagation characteristics are abnormal with seismic wave energy dissipating, and the slope began to damage after 0.297 g. Figure 12 also shows that the PSHEA of the measuring points (A10, A16, and A18) in the surface slope is larger than that of the measuring points (A2, A7, and A13) inside the slope, resulting in different dynamic responses between the internal slope and surface slope. This indicates that the slope body below the topmost bedding structural plane is the sliding bed, and the surface slope is the potential slip mass. Therefore, according to the analyses of the seismic Hilbert energy, the dynamic failure evolution process of the earthquake-induced landslide mainly includes no seismic damage stage (0.074–0.297 g) and sliding failure stage (0.297–0.446 g).

Analysis of marginal spectrum

To further investigate the position and the seismic failure development process of the slope, the marginal spectrum of the slope was analyzed. Figure 9 shows that the IMF2 and has the apparent characteristics with rich frequency components, large amplitude, and high identification degree; hence, the IMF2 is used to obtain the marginal spectra of the slope. The marginal spectrum of the typical measuring points in the slope can be obtained, as shown in Fig. 13. Figure 13 shows that the marginal spectrum amplitude is much larger in 20–40 Hz, indicating that energy focused on the high-frequency components. In combination with the analytical results in Fig. 8, the high-frequency components mainly induced the local deformation of the slope; hence, the marginal spectrum can be used to identify the dynamic local damage of the slope. The PMSA (peak marginal spectrum amplitude) with elevation is shown in Fig. 14. Figure 14 shows that the PMSA increases with elevation inside the slope from 0.074 to 0.148 g, suggesting that no damage deformation appears inside the slope. However, a sudden decrease between A10 and A16 can be found subject to 0.297 g. The rapid decrease of PMSA suggests that the wave energy cannot propagate completely in the slope, and seismic damage begins to occur near the platform area between A10 and A16. The PMSA between the A13 increases with the elevation inside the slope subject to 0.297 g, but a sudden decrease of PMSA can be found above A18, suggesting that the seismic damage occurred in the surface slope. Figure 14 also shows that PMSA decreases abruptly above the A10 at the slope surface subject to 0.446 g, implying that the seismic damage continues to develop upwards in the surface slope above A10, and dynamic damage appears at the top slope. Particularly, the PMSA of the measuring points in the surface slope

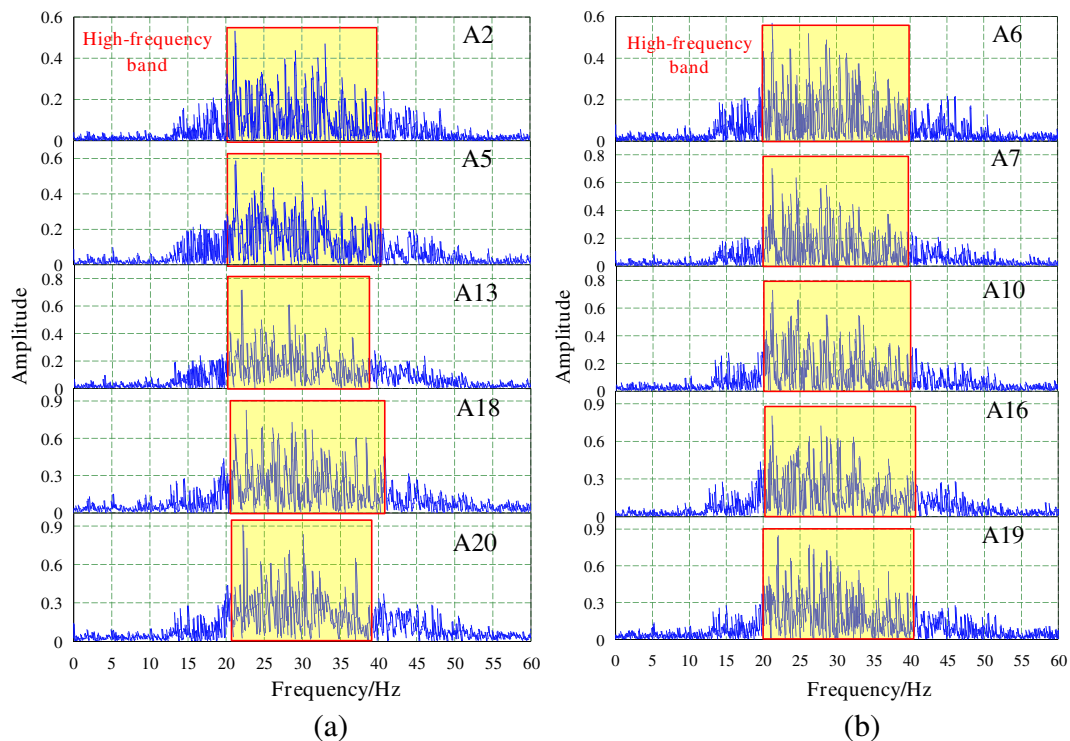


Fig. 13 The marginal spectrum of monitoring points when input in x -direction (0.074 g): a inside the slope; b near the slope surface

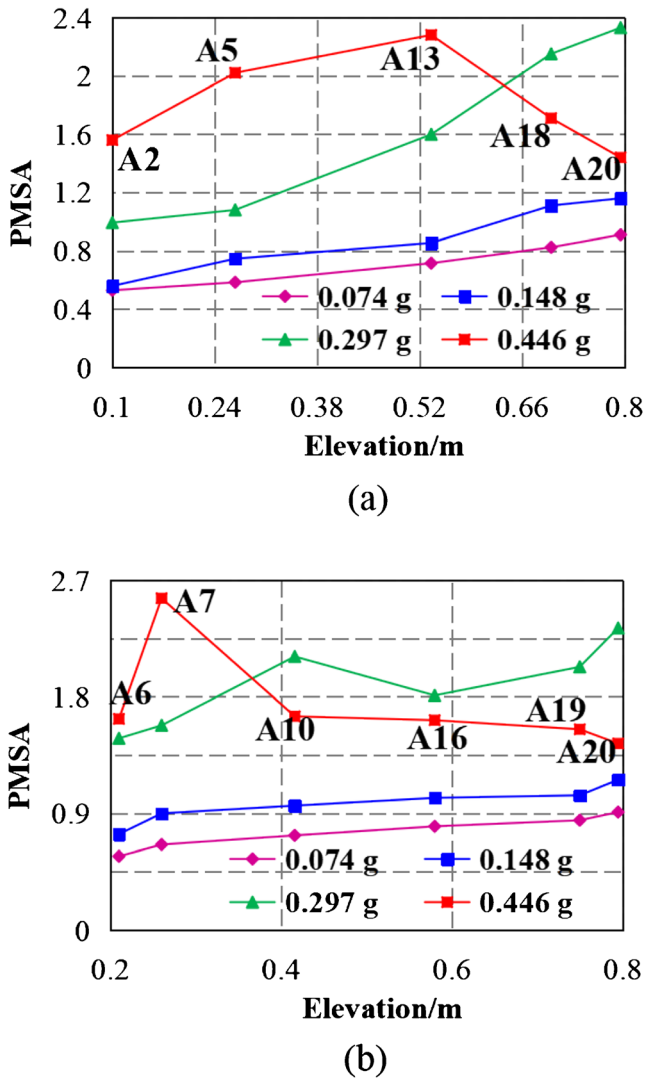


Fig. 14 The change rule of PMSA when input in x -direction: a inside the slope; b near the slope surface

(A10, A16, A18, A19, and A20) under 0.446 g are smaller than that under 0.297 g, which indicates that the surface slope is the main seismic damage area. Additionally, the distribution of PMSA in the slope when input in x and z -directions is shown in Fig. 15. In Fig. 15, the distribution cloud picture of the PFSA is also drawn by using Surfer 10 software. When no dynamic damage appears in the slope, the PMSA shows an increasing trend with the elevation subject to 0.074 g and 0.148 g, suggesting that the wave energy propagation through the slope is regular, and no damage occurs before 0.148 g. However, the PMSA near the platform is smaller than that of the surrounding area when the seismic intensity is 0.297 g, suggesting that the seismic damage occurs at the platform, resulting in the abnormal energy transmission near the platform area. In particular, the PMSA of the surface slope is smaller than that internal slope under 0.446 g, which indicates that the sliding failure of surface slope occurs along the topmost structural plane. Therefore, the seismic damage of the slope can be clarified by analyzing the PMSA distribution (Fig. 15), according to identifying the regions where the energy cannot be transmitted.

In addition, the PMSA with the seismic intensity is shown in Fig. 16. It can be seen that the PMSA of the internal slope (A2, A5, A6, A7, and A13) gradually from 0.074 to 0.446 g (Fig. 16a), indicating that no dynamic damage appears inside the slope under earthquake excitation. The PMSA of the surface slope (A10, A16, A18, A19, and A20) increases from 0.074 to 0.297 g (Fig. 16b), suggesting that no seismic damage appears in the surface slope. But a decrease of PMSA of the surface slope can be found after 0.297 g, suggesting that seismic failure occurs in the surface slope. Combined with Figs. 13, 14, 15, and 16, the seismic damage process of the landslide can be identified as follows: no seismic damage stage (0.074–0.148 g), local damage stage (0.148–0.297 g), and sliding failure stage (0.297–0.446 g). Local seismic damage initiates to occur firstly near the platform under 0.297 g and further continues to expand in the surface slope with the sliding body forming gradually; then, when the earthquake excitation reaches 0.446 g, the surface slope began to slide along the topmost bedding structural plane.

Seismic failure mechanism of the slope using energy-based method

Seismic failure mechanism determines the occurrence and development of slope failure under earthquake excitation (Fan et al. 2017). Figure 17 shows that no large deformation appears in the slope before 0.148 g, and penetrating cracks occur along the joints at the platform area, causing local failure in this area, when it is 0.297 g. When it reaches 0.446 g, all the blocks appear in the surface slope, and the surface slope will slide along the uppermost bedding surface. The seismic damage phenomenon of slope is consistent with the analytical results of marginal spectrum. Moreover, the dynamic failure mechanism of the slope during earthquakes can be interpreted from an energy-based perspective. With the continuous seismic excitation, when the incident wave reaches the slope surface, it will be superimposed on the reflected wave. The Hilbert energy under earthquake action is stored in the surface slope, which is larger than the internal slope. The difference of seismic Hilbert energy between the sliding bed and the sliding body mainly causes different dynamic responses between them, which is an important reason for the dynamic failures in the structural plane. Due to the impact of the structural planes on the distribution of seismic Hilbert energy, the seismic Hilbert energy of the surface slope is larger than that of the internal slope. According to the analyses of the marginal spectrum, the seismic Hilbert energy in the high-frequency components (> 20 Hz) mainly induced the local damage of the slope and initiated the dynamic failure in the middle and crest of the surface slope. Local failure results in the enlargement of pores in the structural planes of surface slope and further leads to the increase of energy dissipation. The seismic Hilbert energy in the 15–17 Hz will magnify the seismic response of the surface slope due to the resonance effect and trigger the overall damage of the surface slope. In the process of shear failure in the structural plane, seismic Hilbert energy is dissipated gradually in the structural plane with increasing seismic intensity. The energy dissipation reaches the largest subject to 0.446 g, resulting in the decrease of the seismic Hilbert energy of the surface slope (Fig. 12), which leads to that the surface slope slides along the topmost structural plane.

In addition, the slope surface displacement and the layered removal of the damaged model are used to further verify the seismic failure mode of the slope (Figs. 18 and 19). By selecting

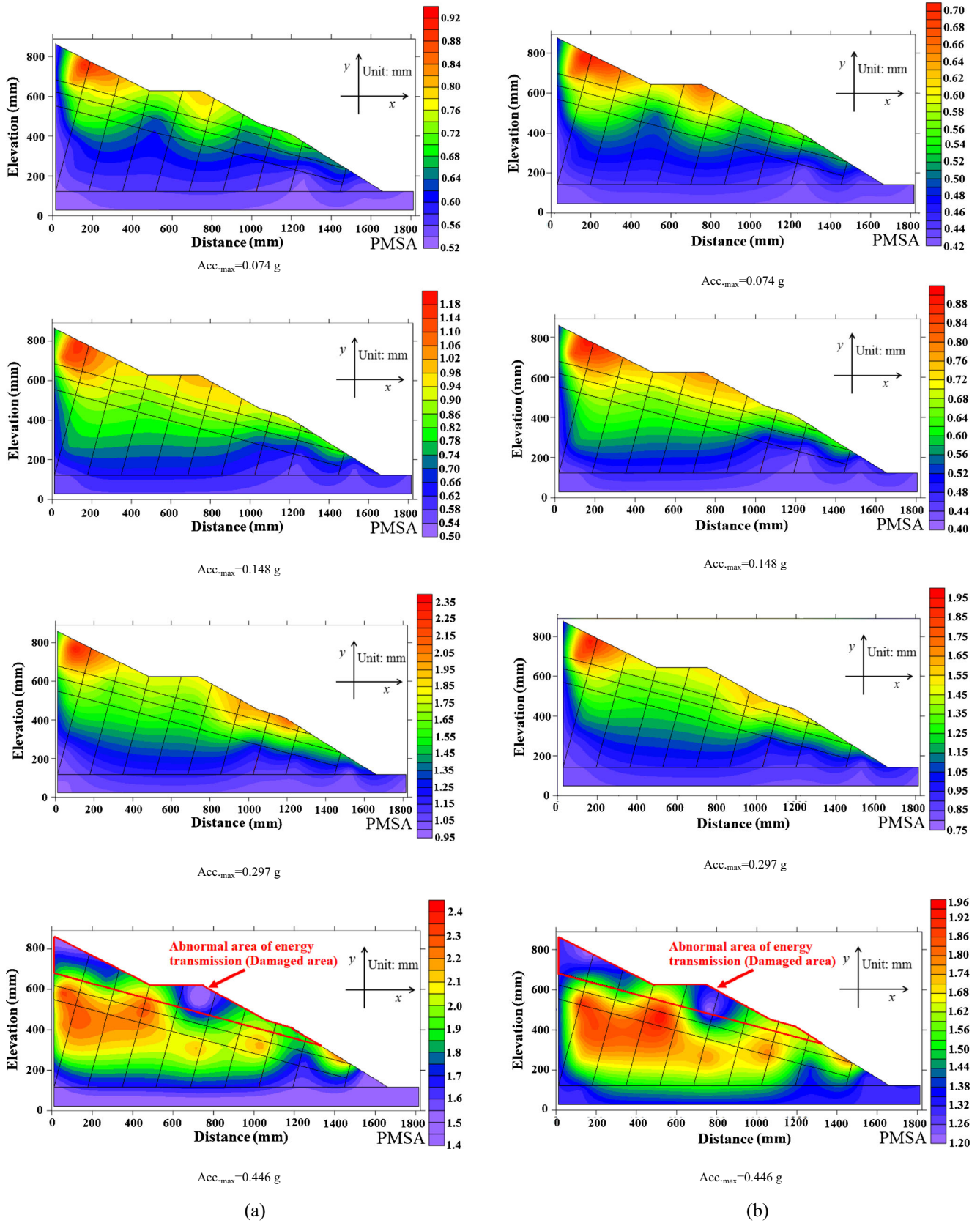


Fig. 15 Distribution of PMSA under different seismic intensities: a input in x-direction; b input in z-direction

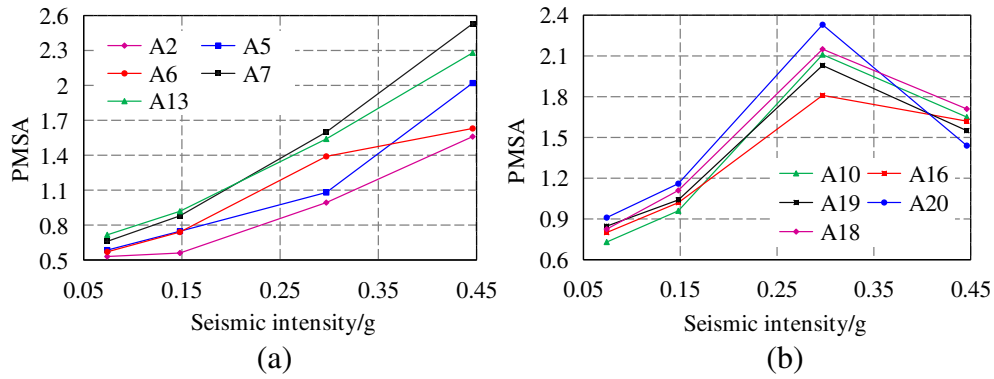


Fig. 16 The change rule of PMSA with seismic intensity when input in *x*-direction: **a** inside the slope; **b** near the slope surface

optical measuring points at different elevations of the slope surface, the displacement of the slope surface is analyzed, as shown in Fig. 18. The points are located in the middle section of the slope surface, and the surface displacement is measured by the XTDIC 3D optical deformation measurement system. Figure 18 shows that the slope surface displacement is mainly concentrated above the topmost bedding structural plane, while the surface displacement below it is very small, which indicates that the surface slope is mainly deformed and damaged area. Figure 19 shows that when the damaged model is dismantled, it is obvious that the slope body below the superstructure surface is not damaged, which also indicates that only the surface slope body is damaged. Therefore, the topmost bedding structural plane is the slip surface, and the surface slope body is a sliding body.

In addition, taking the measuring points in the sliding body (A10 and A20) and in the sliding bed (A4 and A13) as examples, the difference in the acceleration-time histories (A10-A4 and A20-A13) is shown in Fig. 20. An obvious difference can be identified between sliding body and sliding bed. Before the slip plane is formed, when the seismic intensity is less than 0.297 g, the acceleration differences of A20-A13 are larger than those of A10-A4, suggesting that a nonuniform seismic response in the slip mass and the seismic response of the slope crest is much larger. The differences in acceleration between the slip mass and the sliding bed increase gradually with the seismic intensity, suggesting that the corresponding deformation difference between them increases. The slip surface forms subject to 0.446 g, and the acceleration differences of A20-A13 and A10-A4 are similar, implying that the seismic response in the slip mass tends to be stable after the

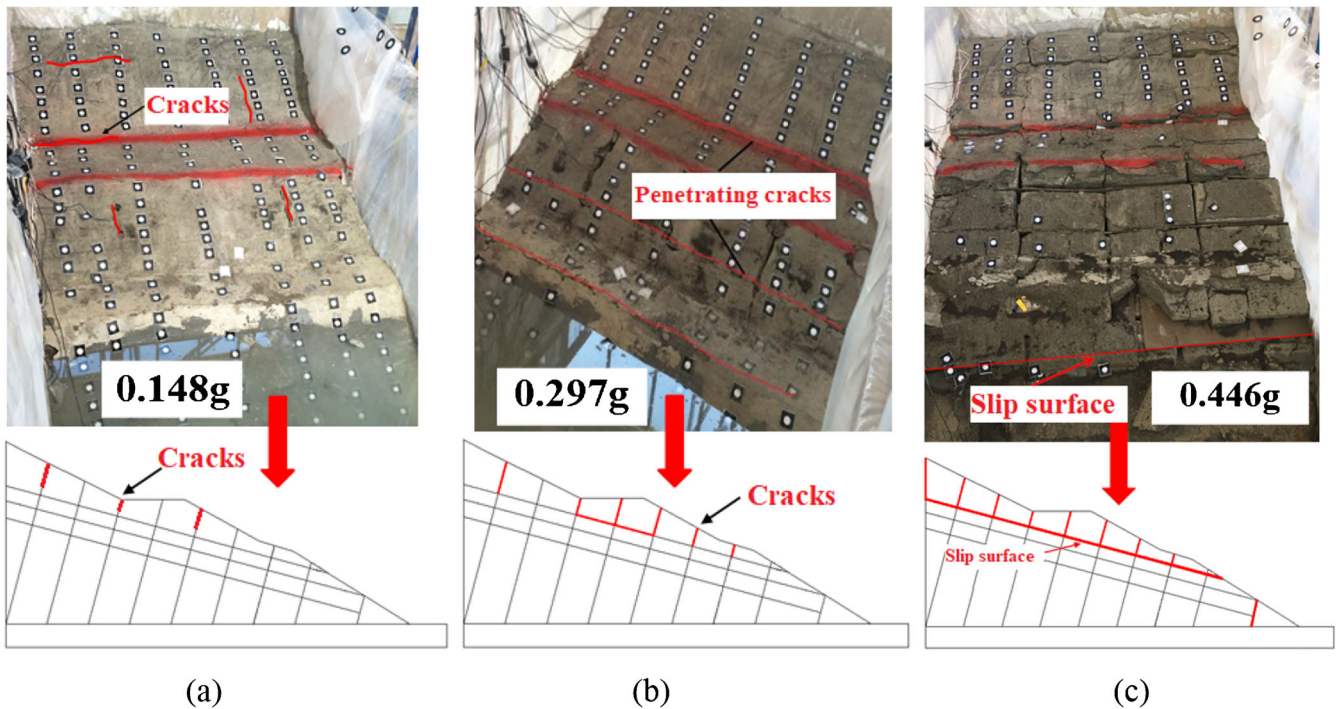


Fig. 17 Dynamic failure phenomenon of the under different seismic intensity: **a** 0.148 g; **b** 0.297 g; **c** 0.446 g

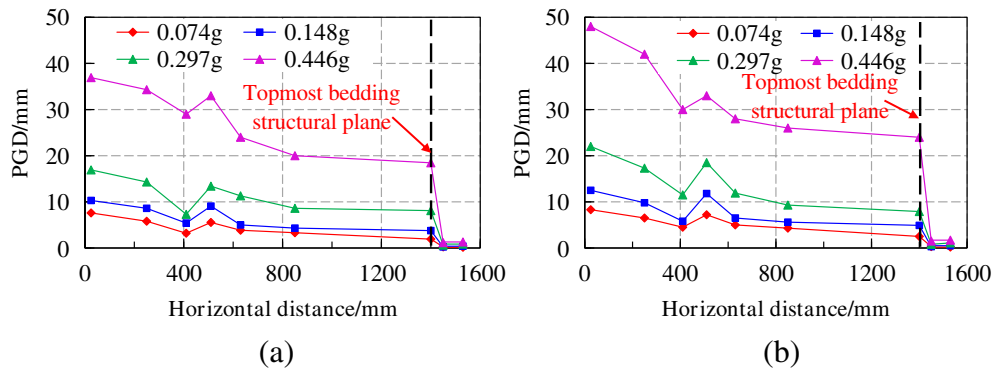


Fig. 18 Displacement of the slope surface when input AS wave: **a** input in z -direction; **b** input in x -direction

formation of the slip surface. This phenomenon further verifies the previous conclusion that the difference of seismic response between the sliding bed and the slip mass mainly causes the occurrence of the landslide using energy-based method.

Discussion

To verify the results of energy-based method, the Fourier spectral ratio was used to clarify the dynamic response of the slope as well. The point A2 at the bedrock is selected as the reference point. Taking the input horizontal 0.074 g AS wave as an example, the Fourier spectrum ratio curves of four measuring points (A6, A10, A16, and A20) are shown in Fig. 21. Taking the first natural frequency (f_2) as an example, the change rule of peak Fourier spectral ratio amplitude (PFSRA) with seismic intensity is shown in Fig. 22. Figure 22 shows that the PFSRA presented a gradual increase before 0.297 g and a decrease after 0.297 g. This indicates that after 0.297 g, the seismic response of the slope changed greatly, and the slope began to be damaged. By comparing the analysis results of the energy-based method (Figs. 12 and 16), PFSRA and PHSA have the similar change rules, which indicates that Fourier spectrum ratio and Hilbert energy spectrum can better reflect the overall deformation of the slope. Therefore, the

Hilbert energy spectrum mainly reflects the overall energy transmission characteristics of the slope; however, it is difficult to accurately analyze the specific damage locations of slope from the perspective of local damage, because the seismic Hilbert energy spectrum is doped with many frequency components of all IMF energy spectra. Compared with the seismic Hilbert energy spectrum, the marginal spectrum represents a certain Hilbert energy spectrum of the IMF with a high identification degree. The marginal spectrum can better reflect the transmission characteristics of energy and clearly identify the local seismic damage.

Conclusions

An energy-based identification method of seismic damage of a slate slope with discontinuities was proposed based on HHT and marginal spectrum. Some conclusions can be drawn.

1. The HHT and its marginal spectrum are feasible to clarify changes of seismic Hilbert energy in the seismic failure mechanism of the slope. Elevation has a magnifying effect on the energy propagation of seismic wave. The PSHEA and PMSA increase with the elevation and reach the maximum at slope crest. The bedding structural plane has a certain aggregation

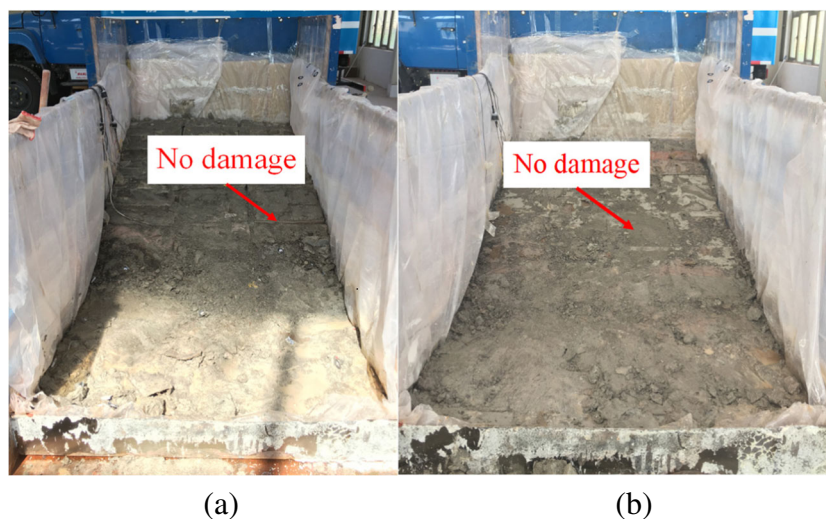


Fig. 19 Removal of the first and second layered slope: **a** after the removal of the first layer; **b** after the removal of the second layer

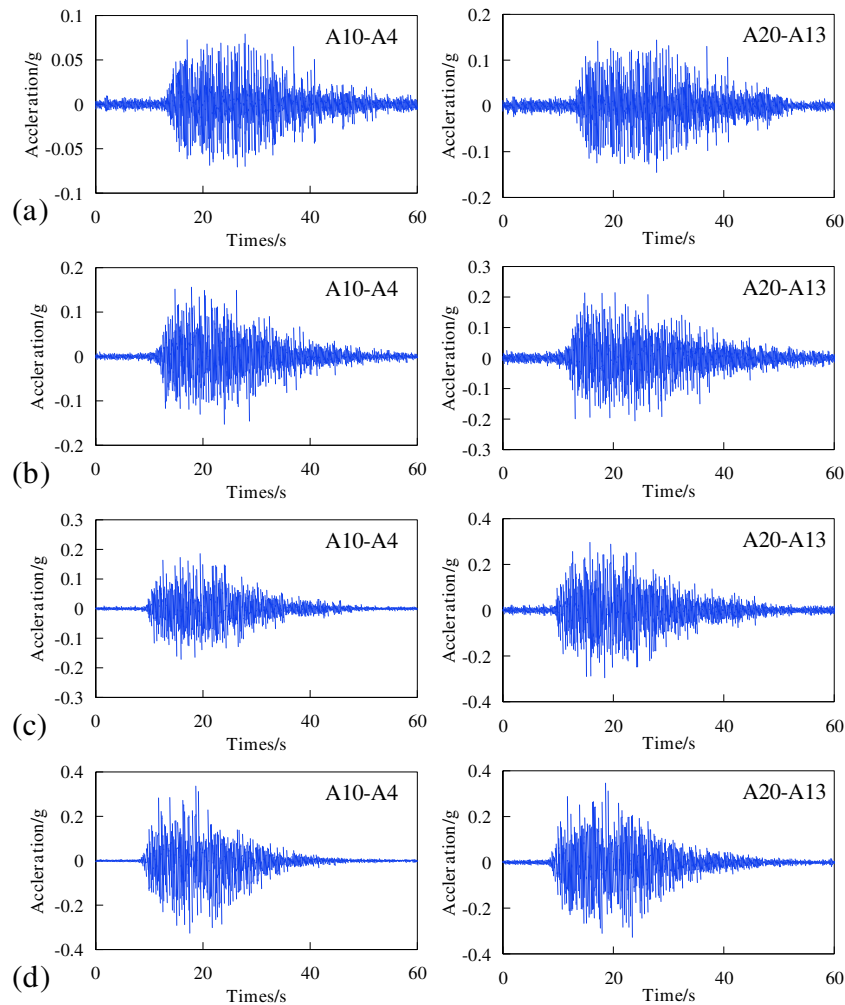


Fig. 20 Acceleration difference between the sliding mass and the sliding bed in the tests

and amplification effect on the seismic wave energy. The spectral amplitude near the PSHEA of the surface slope is significantly amplified apparently. The amplitude of the seismic Hilbert energy spectrum and the marginal spectrum are the

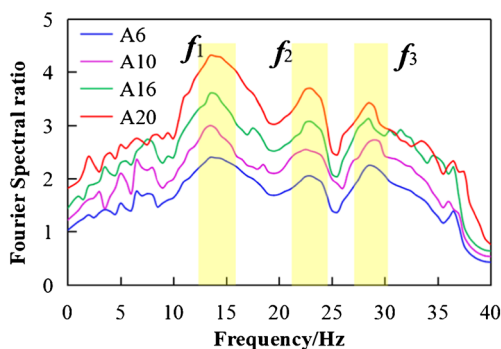


Fig. 21 The Fourier spectrum ration curves when input AS wave in *x*-direction (0.074 g)

largest in the low-frequency (15–17 Hz) and the high-frequency components (> 20 Hz), respectively. The Hilbert energy spectrum and marginal spectrum can be used to identify the overall deformation and local deformation, respectively. The seismic Hilbert energy in the slip mass is larger than the Hilbert energy in the sliding bed, and the difference of seismic Hilbert energy between the sliding bed and the sliding body mainly causes the occurrence of the landslide.

2. The analyses of seismic Hilbert energy spectrum show that the dynamic failure evolution process of the landslide mainly includes no seismic damage stage (0.074–0.297 g) and sliding failure stage (0.297–0.446 g). The analyses of the marginal spectrum suggest that the seismic failure developing process of the slope mainly includes no seismic damage stage (0.074–0.148 g), local damage stage (0.148–0.297 g), and sliding failure stage (0.297–0.446 g). Compared with Hilbert energy spectrum, the marginal spectrum is obtained from the IMF with a high identification degree and can better reflect the transmission characteristics of energy and identify the destructive development process of the landslide from a local perspective.

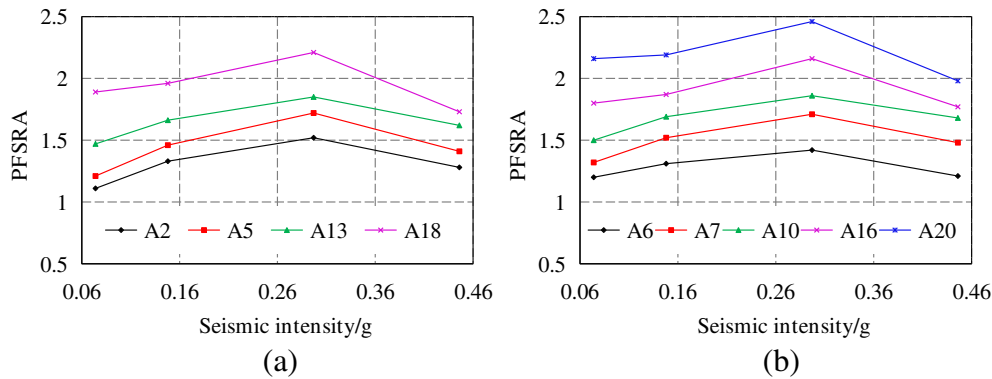


Fig. 22 The peak values of the Fourier spectrum ratios during the first natural frequency (f_2) when input A5 wave in x -direction: **a** inside the slope; **b** near the slope surface

- The dynamic failure mechanism of the slope can be identified from the energy-based perspective by using seismic Hilbert energy. Due to much more seismic Hilbert energy dissipating in the topmost structural plane during the formation of the slip surface, local damage initiates to occur firstly at the platform under 0.297 g, and further continues to expand with the sliding body forming gradually; then, the surface slope began to slide along the topmost bedding structural plane subject to 0.446 g. The seismic Hilbert energy in the high-frequency components mainly induces the local deformation of the surface slope. When the local deformation of the surface slope accumulates to a certain amount, the surface slope gradually forms a sliding body with the development of dynamic failure, and the seismic Hilbert energy in the low-frequency components further promotes the occurrence of the landslide.

However, the model is a simplified model of a slope with two perpendicular, persistent discontinuity sets, which is an unfavorable kinematic setting and is also representative only of specific cases. Moreover, the proposed energy-based method not considers the seismic Hilbert energy distribution characteristics in the time domain, resulting in the difficulty of determining the specific failure time of the landslide under earthquake excitation. The seismic failure mechanism of landslides with complex geological structures should be further investigated based on the energy-based method by using HHT and marginal spectrum.

Funding information

This work was supported by the National Postdoctoral Program for Innovative Talent of China (BX20200191), the National Key R&D Program of China (Grant No. 2018YFC1504902), and the National Natural Science Foundation of China (Grant Nos. 51522903, 51479094, 41772246).

References

Cao L, Zhang J, Liu F, Yang L, Wu J, Wang Z (2017) Dynamic response and failure mode of the complex site with tilting strongly weathered layer and local slopes. *Chin J Rock Mech Eng* 36(9):2238–2250

- Chang KJ, Taboada A, Chan YC, Dominguez S (2006) Post-seismic surface processes in the Jiufengershan landslide area, 1999 Chi-Chi earthquake epicentral zone, Taiwan. *Eng Geol* 86(2–3):102–117. <https://doi.org/10.1016/j.enggeo.2006.02.014>
- Chen ZL, Xu Q, Hu X (2013) Study on dynamic response of the “dualistic” structure rock slope with seismic wave theory. *J Mt Sci* 10(6):996–1007. <https://doi.org/10.1007/s11629-012-2490-7>
- Chen BR, Feng XT, Li QP, Luo RZ, Li S (2015) Rock burst intensity classification based on the radiated energy with damage intensity at Jinping II hydropower station, China. *Rock Mech Rock Eng* 48(1):289–303. <https://doi.org/10.1007/s00603-013-0524-2>
- Chen Z, Song DQ, Hu C, Ke YT (2020) The September 16, 2017, Linjiabang landslide in Wanyuan County, China: preliminary investigation and emergency mitigation. *Landslides* 17:191–104. <https://doi.org/10.1007/s10346-019-01309-1>
- Fan G, Zhang J, Wu J, Yan K (2016) Dynamic response and dynamic failure mode of a weak intercalated rock slope using a shaking table. *Rock Mech Rock Eng* 49(8):1–14. <https://doi.org/10.1007/s00603-016-0971-7>
- Fan G, Zhang LM, Zhang JJ, Ouyang F (2017) Energy-based analysis of mechanisms of earthquake-induced landslide using Hilbert–Huang transform and marginal spectrum. *Rock Mech Rock Eng* 50(4):1–17. <https://doi.org/10.1007/s00603-017-1245-8>
- Fan G, Zhang LM, Li XY, Fan RL, Zhang JJ (2018) Dynamic response of rock slopes to oblique incident SV waves. *Eng Geol* 247:94–103. <https://doi.org/10.1016/j.enggeo.2018.10.022>
- Han WQ, Ying L, Gu AJ, Yuan FG (2016) Damage modes recognition and Hilbert–Huang transform analyses of CFRP laminates utilizing acoustic emission technique. *Appl Compos Mater* 23(2):1–24. <https://doi.org/10.1007/s10443-015-9454-3>
- Huang R, Li W (2014) Post-earthquake landsliding and long-term impacts in the Wenchuan earthquake area, China. *Eng Geol* 182:111–120. <https://doi.org/10.1016/j.enggeo.2014.07.008>
- Huang NE, Shen Z, Long SR, Wu MC, Shih HH, Zheng QA, Yen NC, Tung CC, Liu HH (1998) The empirical mode decomposition and Hilbert spectrum for nonlinear and non-stationary time series analysis. *Proc R Soc A* 454:903–995. <https://doi.org/10.1098/rspa.1998.0193>
- Huang NE, Shen Z, Long SR (1999) A new view of nonlinear water waves: the Hilbert spectrum. *Annu Rev Fluid Mech* 31(1):417–457. <https://doi.org/10.1146/annurev.fluid.31.1.417>
- Jia J (2008) An efficient nonlinear dynamic approach for calculating wave induced fatigue damage of offshore structures and its industrial applications for lifetime extension. *Appl Ocean Res* 30(3):189–198. <https://doi.org/10.1016/j.apor.2008.09.003>
- Jiang M, Jiang T, Crosta GB, Shi Z, Chen H, Zhang N (2015) Modeling failure of jointed rock slope with two main joint sets using a novel DEM bond contact model. *Eng Geol* 193:79–96. <https://doi.org/10.1016/j.enggeo.2015.04.013>
- Kokusho T, Ishizawa T, Koizumi K (2011) Energy approach to seismically induced slope failure and its application to case histories. *Eng Geol* 122:115–128. <https://doi.org/10.1016/j.enggeo.2011.03.019>
- Kokusho T, Koyanagi T, Yamada T (2014) Energy approach to seismically induced slope failure and its application to case histories — supplement. *Eng Geol* 181:290–296. <https://doi.org/10.1016/j.enggeo.2014.08.019>
- Lenti L, Martino S (2012) The interaction of seismic waves with step-like slopes and its influence on landslide movements. *Eng Geol* 126:19–36. <https://doi.org/10.1016/j.enggeo.2011.12.002>

- Li J, Law SS, Ding Y (2012) Substructure damage identification based on response reconstruction in frequency domain and model updating. *Eng Struct* 41(3):270–284. <https://doi.org/10.1016/j.engstruct.2012.03.035>
- Meng Q, Zhang M, Han L, Pu H, Nie T (2016) Effects of acoustic emission and energy evolution of rock specimens under the uniaxial cyclic loading and unloading compression. *Rock Mech Rock Eng* 49(10):1–14. <https://doi.org/10.1007/s00603-016-1077-y>
- Munoz H, Taheri A, Chanda EK (2016) Fracture energy-based brittleness index development and brittleness quantification by pre-peak strength parameters in rock uniaxial compression. *Rock Mech Rock Eng* 49(12):4587–4606. <https://doi.org/10.1007/s00603-016-1071-4>
- Pai PF, Palazotto AN (2008) HHT-based nonlinear signal processing method for parametric and non-parametric identification of dynamical systems. *Int J Mech Sci* 50(12):1619–1635. <https://doi.org/10.1016/j.ijmecsci.2008.10.001>
- Peláez JA, Delgado J, Casado CL (2005) A preliminary probabilistic seismic hazard assessment in terms of arias intensity in southeastern Spain. *Eng Geol* 77(1):139–151. <https://doi.org/10.1016/j.enggeo.2004.09.002>
- Peng R, Ju Y, Wang JG, Xie H, Gao F, Mao L (2015) Energy dissipation and release during coal failure under conventional triaxial compression. *Rock Mech Rock Eng* 48(2):509–526. <https://doi.org/10.1007/s00603-014-0602-0>
- Qi S, Xu Q, Lan H, Zhang B, Liu J (2010) Spatial distribution analysis of landslides triggered by 2008.5.12 Wenchuan earthquake, China. *Eng Geol* 116(1–2):95–108. <https://doi.org/10.1016/j.enggeo.2010.07.011>
- Roveri N, Carcaterra A (2012) Damage detection in structures under traveling loads by Hilbert–Huang transform. *Mech Syst Signal Process* 28:128–144. <https://doi.org/10.1016/j.ymssp.2011.06.018>
- Song D, Che A, Zhu R, Ge X (2018a) Dynamic response characteristics of a rock slope with discontinuous joints under the combined action of earthquakes and rapid water drawdown. *Landslides* 15(6):1109–1125. <https://doi.org/10.1007/s10346-017-0932-6>
- Song D, Che A, Zhu R, Ge X (2018b) Seismic stability of a rock slope with discontinuities under rapid water drawdown and earthquakes in large-scale shaking table tests. *Eng Geol* 245:153–168. <https://doi.org/10.1016/j.enggeo.2018.08.011>
- Song D, Chen J, Cai J (2018c) Deformation monitoring of rock slope with weak bedding structural plane subject to tunnel excavation. *Arab J Geosci* 11(11):251. <https://doi.org/10.1007/s12517-018-3602-7>
- Song D, Che A, Zhu R, Ge X (2019) Natural frequency characteristics of rock masses containing a complex geological structure and their effects on the dynamic stability of slopes. *Rock Mech Rock Eng* 52:4457–4473. <https://doi.org/10.1007/s00603-019-01885-7>
- Song D, Chen Z, Hu C, Ke Y, Nie W (2020) Numerical study on seismic response of a rock slope with discontinuities based on the time-frequency joint analysis method. *Soil Dyn Earthq Eng* 133:106112. <https://doi.org/10.1016/j.soildyn.2020.106112>
- Veltcheva A, Soares CG (2016) Nonlinearity of abnormal waves by the Hilbert–Huang transform method. *Ocean Eng* 115:30–38. <https://doi.org/10.1016/j.oceaneng.2016.01.031>
- Wang Z, Cheng F, Chen Y, Cheng W (2013) A comparative study of delay time identification by vibration energy; analysis in millisecond blasting. *International Journal of Rock Mechanics & Mining Sciences* 60(8):389–400. <https://doi.org/10.1016/j.ijrmms.2012.12.032>
- Wu W, Li JC, Zhao J (2014) Role of filling materials in a P-wave interaction with a rock fracture. *Eng Geol* 172(8):77–84. <https://doi.org/10.1016/j.enggeo.2014.01.007>
- Xu C, Xu XW, Yu GH (2013) Landslides triggered by slipping-fault-generated earthquake on a plateau: an example of the 14 April 2010, Ms 7.1, Yushu, China earthquake. *Landslides* 10(4):421–431. <https://doi.org/10.1007/s10346-012-0340-x>
- Yin YP, Wang F, Ping S (2009) Landslide hazards triggered by the 2008 Wenchuan earthquake, Sichuan, China. *Landslides* 6(2):139–152. <https://doi.org/10.1007/s10346-009-0148-5>
- Zhang YP (2006) HHT analysis of blasting vibration and its application. PhD thesis, Central South University, Changsha, China
- Zhang F, Huang X (2018) Trend and spatiotemporal distribution of fatal landslides triggered by non-seismic effects in China. *Landslides* 15(8):1663–1674. <https://doi.org/10.1007/s10346-018-1007-z>

D. Song · X. Liu (✉) · J. Huang · J. Zhang

Department of Hydraulic Engineering, State Key Laboratory of Hydrosience and Engineering, Tsinghua University, Beijing, 100084, China
Email: xiaoli.liu@tsinghua.edu.cn